Methylamine Adsorption on and Desorption from Si(100)

April J. Carman, Linhu Zhang, Jason L. Liswood, and Sean M. Casey*

Department of Chemistry and Chemical Physics Program, MS 216, University of Nevada, Reno, Nevada 89557

Received: June 13, 2002; In Final Form: December 23, 2002

The adsorption of several simple methylamines on the Si(100)-(2 × 1) surface has been investigated using Auger electron spectroscopy (AES), thermal desorption spectroscopy (TDS), low-energy electron diffraction, and computational modeling. Both methylamine and dimethylamine appear to undergo mostly dissociative adsorption on this surface at room temperature, although trapping into a molecular adsorption well appears to occur to a limited extent for both molecules. Trimethylamine appears to undergo mostly molecular adsorption on this surface. These results are in agreement with recent computational, infrared, and photoemission spectroscopic studies of these systems. By comparison to the AES results from the adsorption of methyl iodide on Si(100), it was concluded that the surface saturation coverage of trimethylamine on Si(100) is 0.26 monolayers, consistent with the photoemission results, while both methylamine and dimethylamine appear to saturate at about 0.48 monolayers. TDS reveals parent desorption channels for all three of these molecules, as well as competing surface decomposition channels. The adsorption energies obtained from computational treatments of these systems are consistent with the experimentally derived values.

I. Introduction

The chemistry of semiconductor surfaces is of considerable importance to modern science and technology. Silicon surface chemistry, in particular, has received extensive attention because of this material's technological utility.[1−7] The reactivity of these surfaces is strongly dependent on the electronic environment of the surface atoms, which to a large extent is determined by the geometrical arrangement of the atoms at the surface. The (100) surface of silicon, for example, undergoes a 2 × 1 reconstruction, resulting in the formation of rows of silicon surface dimers.[8−12] The silicon atoms in these surface dimers are bound to each other by a relatively strong σ-type bond and a weak π-type bond, and each atom in the dimer is also bound to two other silicon atoms underneath it in the bulk. These silicon dimers on the (100) surface thus appear to have an electronic structure similar to that of a disilene (a compound with a Si═Si bond) and might be expected to undergo chemistry that is analogous to the chemistry of disilenes.

The silicon π-bonds in disilenes are susceptible to 1,2-addition reactions across the double bond, especially with active hydrogen compounds such as alcohols.[13] The overall mechanism for these reactions is thought to be nucleophilic attack by lone-pair electrons of the polar incident species on one of the silicon atoms, followed by hydrogen transfer to the other silicon atom.[14] These types of reagents,[15−21] as well as amines,[7,22−26] have been observed to undergo addition reactions with silicon surface dimer π-bonds. In the case of amines, the initial interaction with the surface is thought to occur via a nucleophilic attack by the nitrogen lone-pair on one of the silicon atoms in the dimer.[23−26] The surface dimers can accommodate this type of interaction in their buckled form, which has an electron distribution that is shifted from the π-like orbital of the symmetric dimer to a zwitterionic-type distribution with the lower silicon atom of the buckled pair having a partial positive charge and the upper atom having a partial negative charge.[27] The partial positive charge on the lower silicon atom stabilizes the "dative bond" resulting from the nucleophilic attack of the nitrogen lone pair on this atom. Further reaction with the surface can then occur, for ammonia and primary and secondary amines, by hydrogen (or proton)[25] transfer to the electronegative upper silicon atom of the buckled dimer, in a manner similar to the 1,2-addition of active hydrogen compounds to stable disilenes. Tertiary amines, which do not have this channel available, can become trapped in the dative-bond well, forming a quaternary ammonium-type adduct.[23−26]

The interactions of the methyl-, dimethyl-, and trimethylamine molecules with the silicon surface have been studied previously by infrared and photoemission spectroscopies and by computational methods.[23−26] Infrared spectroscopy results demonstrate that adsorption of methyl- and dimethylamine occurs through N−H bond cleavage with subsequent attachment of the hydrogen atom to a silicon atom.[23,24] This reaction is not observed for trimethylamine. Photoemission results comparing dimethylamine to trimethylamine indicate that trimethylamine is mainly adsorbed on the silicon surface in a quaternary ammonium-like state (the datively bonded state); this state is not observed in the case of dimethylamine adsorption.[24] These results are consistent with computational studies[23−26] of these reactions carried out on Si_9H_{12} clusters that are meant to mimic the Si(100) surface. These studies, carried out using density functional theory (DFT),[28,29] predict that the N−H bond cleavage channel is kinetically favored relative to the thermodynamically favored N−C bond cleavage channel.[23−26] The barrier to N−H bond cleavage (out of the initial datively bonded molecularly adsorbed state) is predicted to be below the energy of the free molecule and the surface, while that of N−C bond cleavage is above this asymptotic level. This is consistent with the experimental data, which indicate that both methyl- and dimethylamine react via N−H cleavage, while trimethylamine remains mostly trapped in the datively bonded well, unable to overcome the N−C bond cleavage barrier at room temperature.

In this study, we report on further investigation of the adsorption and reaction of these methylamines on the Si(100)-

* To whom correspondence should be addressed. Phone: (775) 784-4133. Fax: (775) 784-6804. E-mail: scasey@chem.unr.edu.

10.1021/jp021419+ CCC: $25.00
Published on Web 05/16/2003

(2 × 1) surface to more fully probe the reaction energetics for these molecules. We have used low-energy electron diffraction (LEED), Auger electron spectroscopy (AES), and thermal desorption spectroscopy (TDS) to probe the interaction of these molecules with the surface experimentally and ab initio and DFT computations to explore the available reaction pathways, including the previously unreported C−H cleavage pathway. Thermal desorption from the "dative-bond" molecular adsorption well is observed for all of the methylamine species studied. Results from these current studies complement the photoemission, multiple internal reflection Fourier transform infrared (MIR−FTIR) spectroscopic, and computational studies recently reported on these systems[23−26] and provide further detail about the energetics of these surface reactions.

II. Experimental and Theoretical Methods

The amine adsorption and decomposition experiments were carried out in a stainless steel ultrahigh vacuum (UHV) chamber that has been described in detail elsewhere.[22] The chamber is equipped with rear-view four-grid LEED optics that are utilized in retarding-field analysis mode for the recording of Auger electron spectra. The chamber is also equipped with a cold-cathode argon ion gun for sample cleaning and a quadrupole mass spectrometer (QMS) for residual gas analysis and for thermal desorption studies. The Si(100) single-crystal wafers (arsenic- or phosphorus-doped, 1−20 Ω·cm, ± 0.5°) used in this work were 0.2−0.6 mm thick and were mechanochemically mirror polished on one side (Polishing Corporation of America [PCA] or Virginia Semiconductor [VS]). Prior to introduction into the chamber, samples were cut to between 2.5 and 5.0 cm^2 and were cleaned in one of two ways. PCA samples were either etched ex situ to provide an oxide surface following literature recipes[30] and then annealed in the vacuum chamber to obtain a clean silicon surface or subjected to a series of argon sputtering and annealing cycles to provide a clean silicon surface.[22] The VS samples usually yielded clean surfaces after annealing in a vacuum with no additional sputtering or etching steps required. The surface structure and cleanliness after the cleaning cycles were confirmed using AES and LEED. Samples were always cleaned and annealed after any AES or LEED probing before any subsequent dosing. Sample temperatures were measured using a tungsten−5% rhenium vs tungsten−26% rhenium (type-C) thermocouple junction spot-welded to the tantalum backing plate immediately adjacent to the sample. Temperatures were also calibrated against desorption temperatures for the H_2 and SiO desorption products from adsorption of water,[31] H_2 and NH_3 desorption products from ammonia adsorption,[32] and H_2 and C_4H_8 desorption products from the adsorption of *cis*-2-butene on the Si(100) surface.[33] Anhydrous ammonia (Scott Specialty Gases, 99.99%), methylamine (Matheson, 99.5%), d_3-methylamine (CD_3NH_2, Isotec Inc., 99%), dimethylamine (Matheson, 99.5%), and trimethylamine (Aldrich, 99%) were stored in stainless steel lecture or reagent bottles and used without further purification prior to dosing through a variable stainless steel leak valve. All doses were performed with the sample held in the 300−350-K temperature range unless otherwise noted. Exposures are reported in langmuirs (1 langmuir = 1×10^{-6} Torr·s), using the uncorrected pressure reading from a nude ion gauge located in the UHV chamber.

To gain further physical insight into the available reaction pathways for these molecules on the Si(100) surface, we have used ab initio molecular orbital calculations along with DFT to study amine physisorption and chemisorption on Si_9H_{12} single-dimer[34] and $Si_{21}H_{20}$ triple-dimer silicon clusters.[35] The ab initio molecular orbital calculations were carried out on these systems either at the Hartree−Fock (HF) level of theory[36] or using DFT at the B3LYP level of theory[37,38] for geometry optimizations using the Gaussian 98 program package.[39] None of the geometrical parameters describing the cluster or adsorbate were fixed during the optimization calculations. The basis sets for these calculations varied and included double-ζ Gaussian-type basis sets with polarization functions added to the silicon atoms or heavy atoms [the 3-21G(d) basis set or 6-31G(d) basis set, respectively, in Gaussian notation],[40−44] double-ζ Gaussian-type basis sets with diffuse functions and polarization functions added to the heavy atoms [the 6-31+G(d) basis set, in Gaussian notation], and triple-ζ basis sets with diffuse and polarization functions added to heavy atoms and polarization functions added to hydrogen atoms [the 6-311+G(2d,p) basis set, in Gaussian notation].[45−47] Vibrational frequencies were calculated[48,49] at the same level of theory as the optimizations for minima and transition states only for the single-dimer cluster optimized structures to verify the assignment of these stationary points. Frequency calculations were not performed on triple-dimer cluster stationary points; classification of a stationary point as a minimum or a transition state in this case was made on the basis of a comparison to the single-dimer cluster results. The intrinsic reaction coordinates (IRCs)[50,51] between the transition states and minima were mapped only in the single-dimer cluster cases either by fixing the positions of all of the cluster atoms except for the "surface dimer" and the adsorbate at their transition state values or by allowing all atoms to relax. The result from the first method is convergence of the reaction coordinate calculation to a stationary point that is higher in energy than the true relaxed-cluster minimum that can be obtained by the second method. This approach can provide an approximation to the intrinsic reaction coordinate (that would really include cluster relaxation) at a substantial savings in computational effort. Adsorption (following the free molecule + cluster into the molecularly adsorbed well) reaction coordinates were followed by fixing the approach angles of the molecule to be close to normal to the surface dimer. Single-point energies for single- and triple-dimer cluster minima and transition states were calculated at the optimized geometries using DFT at the B3LYP level of theory and using 6-311+G-(2d,p) basis sets. Zero-point vibrational corrections were made to all reported single-point energies (for both single- and triple-dimer calculations) using the values calculated for the single-dimer optimized cluster geometries.[52]

III. Results and Discussion

A. Computational Results. Figure 1 shows a schematic potential energy curve from the computational results (IRC calculations) for the interaction of the ammonia molecule with a silicon cluster that is meant to model the Si(100)-(2 × 1) surface, as is outlined in section II. Ammonia has been extensively studied in the past,[32,52−59] and in this case is used as a calibration system to assess the quality of the computational approaches to be employed for the amines, because ammonia and the amines are expected to interact similarly with the surface, initially, at least. As has been discussed in detail elsewhere,[52−59] the ammonia molecule initially interacts with the surface by formation of a dative bond via donation of the nitrogen lone pair to one of the surface dimer silicon atoms, followed by NH bond cleavage and transfer of a hydrogen atom to the other silicon atom in the dimer. This yields NH_2 and H species bound to adjacent silicon atoms of a surface dimer, and results in one ammonia molecule adsorbed per dimer. Table 1

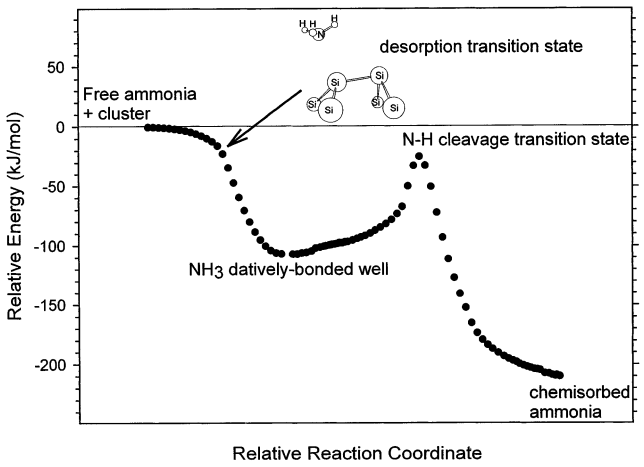

Figure 1. Schematic diagram of the interaction of an ammonia molecule with the Si_9H_{12} cluster model of the Si(100)-(2 × 1) surface. The reaction energetics shown are from intrinsic reaction coordinate calculations at the HF/3-21G(d) level, as described in section II of the text, scaled to the results from the higher level single-point calculations at the stationary points (see Table 1). The arrow points to the transition state for desorption, as discussed in section III.C of the text. For clarity, only the top six silicon atoms of the cluster are shown. The horizontal line represents the energy of the free ammonia + cluster asymptote.

TABLE 1: Comparison of Results from the Computational Treatment of Ammonia Adsorption on Si_9H_{12} Single-Dimer and $Si_{21}H_{20}$ Triple-Dimer Clusters as Described in Section II with Previous Experimental and Computational Results

	dative bond well	N−H transition state	N−H well
Single Dimer (Si_9H_{12}) Values (kJ/mol)			
HF/3-21G*	−175	−79	−340
//B3LYP/6-311+G(2d,p)	−80	−23	−219
B3LYP/6-31G*	−103	−43	−232
//B3LYP/6-311+G(2d,p)	−79	−21	−217
B3LYP/6-31+G*	−87	−28	−221
//B3LYP/6-311+G(2d,p)	−79	−21	−217
B3LYP/6-311+G(2d,p)	−79	−21	−217
CBS-4	−95	−26	−222
Mui et al.[23]	−83	−27	−219
Widjaja and Musgrave[55]	−96	−17	−226
Fattal et al.[56]	−138	−75	−314
Loh and Kang[57]	−115	−42	−228
Lee and Kang[58] (slab)	−103	−45	−195
Miotto et al.[59] (slab)	−105	−42	−234
experiment	−109[53,57]	−17[54]	−193[32]
Triple Dimer ($Si_{21}H_{20}$) Values (kJ/mol)			
HF/3-21G*	−219	−87	−338
//B3LYP/6-311+G(2d,p)	−107	−25	−210
Widjaja and Musgrave[55]	−109	−25	−213
Lee and Kang[58] (slab)	−103	−45	−195
Miotto et al.[59] (slab)	−105	−42	−234
experiment	−109[53,57]	−17[54]	−193[32]

shows the computational results for the physisorbed and chemisorbed wells and the transition state between them, referenced to the separated ammonia + cluster energy asymptote, calculated at various levels of theory for both the single-dimer and triple-dimer surface models. This table also compares these results with previously obtained computational[23,52,55−59] and experimental results.[32,53,54]

As can be seen by examination of Table 1, the treatment of this system at the HF/3-21G(d) level alone gives energetics that are in poor agreement with more extensive treatments[23,52,55−59] and with experiment;[32,53,54] however, the geometries obtained by this method appear to be close to those obtained by more extensive treatments, as is seen in Table 2. This table shows selected geometric parameters for this system obtained at various levels of computational treatment, as compared to results from other computational treatments[55] and experiment.[60] As a result of this good geometric agreement, higher level single-point energy calculations (at the B3LYP/6-311+G(2d,p) level) performed at the HF/3-21G(d) optimized geometries appear to give good agreement (within ±2 kJ/mol) with results obtained from higher level optimizations, in both the single-dimer and triple-dimer cluster cases. In the single-dimer cluster case, the DFT methods appear to converge to energies that are in reasonable agreement with experimental values in the case of the NH cleavage well (within 12.5%) and the transition state (within 4 kJ/mol). However, the well depth of the datively bonded state is grossly underestimated (by 30 kJ/mol or about 28%). Some of the interaction energy can be picked up using complete basis set methods (the CBS-4 method,[61] specifically) on the single-dimer cluster model. This treatment provides corrections due to electron correlation and extrapolates the energy to the complete basis set limit. However, even with this treatment,

TABLE 2: Comparison of Computational Results for Selected Geometrical Parameters of Ammonia Reacting with the Si_9H_{12} Single-Dimer and $Si_{21}H_{20}$ Triple-Dimer Clusters Obtained by the Methods Outlined in Section II with Previously Obtained Computational and Experimental Results

	Si_9H_{12}		
parameter	dative-bond well	transition state	chemisorbed well
	HF/3-21G(d)		
Si−Si (Å)	2.352	2.355	2.397
Si−N (Å)	1.959	1.837	1.721
Si−Si−N (deg)	104.8	86.5	118.3
dimer buckle angle (deg)	9.0	5.3	−0.7
	B3LYP/6-31G(d)		
Si−Si (Å)	2.360	2.374	2.416
Si−N (Å)	2.013	1.884	1.754
Si−Si−N (deg)	104.6	85.7	120.2
dimer buckle angle (deg)	10.3	5.9	−0.5
	B3LYP/6-31+G(d)		
Si−Si (Å)	2.358	2.376	2.418
Si−N (Å)	2.011	1.885	1.755
Si−Si−N (deg)	104.0	85.7	119.5
dimer buckle angle (deg)	10.0	5.7	−0.5
	B3LYP/6-311+G(2d,p)		
Si−Si (Å)	2.354	2.373	2.419
Si−N (Å)	2.001	1.871	1.744
Si−Si−N (deg)	104.6	86.3	119.4
dimer buckle angle (deg)	10.1	5.7	−0.6
	$Si_{21}H_{20}$		
parameter	dative-bond well	transition state	chemisorbed well
	HF/3-21G(d)		
Si−Si (Å)	2.370	2.346	2.389
Si−N (Å)	1.945	1.837	1.715
Si−Si−N (deg)	105.5	86.5	117.6
dimer buckle angle (deg)	10.3	5.3	0.4
	Widjaja and Musgrave[55]		
Si−Si (Å)	2.38	2.37	2.41
Si−N (Å)	2.00	1.86	1.74
Si−Si−N (deg)	104	86	119
dimer buckle angle (deg)	13	6	1
	experiment[60]		
Si−Si (Å)			2.8 ± 0.3
Si−N (Å)			1.73 ± 0.03
Si−Si−N (deg)			103 ± 9
dimer buckle angle (deg)			8 ± 8

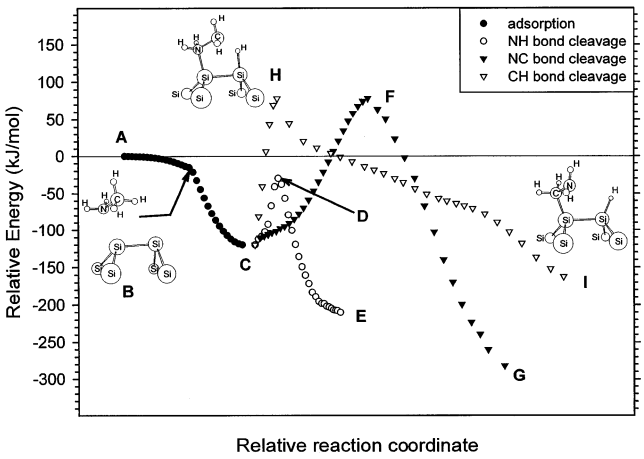

Figure 2. Schematic diagram of reaction pathways available to methylamine adsorbed on the Si_9H_{12} cluster model of the Si(100)-(2 × 1) surface. The values shown are from intrinsic reaction coordinate calculations at the HF/3-21G(d) level, scaled to the results from the higher level single-point calculations at the stationary points (see Table 3). Point A represents the free methylamine + cluster level. Point B is the transition state for desorption (illustrated). Point C is the datively bonded well, point D is the transition state for N−H bond cleavage, point E is the N−H bond cleaved well, point F is the N−C bond cleavage transition state, and point G is the N−C bond cleaved well. Points H and I (illustrated) represent the C−H bond cleavage transition state and well, respectively.

the energetics of the datively bonded well appear to be underestimated. When the triple-dimer cluster model is used, the presence of an extended surface allows for delocalization of the bonding in the dative bond well, as has been discussed by Musgrave and co-workers,[23,52,55] and results in a lowering of the computed well depth, comparing favorably with experiment. Overall, this comparison indicates that the approach outlined in section II, in which geometries and frequencies for the stationary points are computed at the HF/3-21G(d) level, followed by higher level single-point energy computations (typically at the B3LYP/6-311+G(2d,p) level), gives results that are in good agreement with experiment for these systems (in the triple-dimer case) at a reasonable computational expense.

Figure 2 shows a schematic potential energy curve from the computational results for the interaction of the methylamine molecule with the silicon cluster surface model. As has been discussed in section I and elsewhere,[23−25] the methylamine molecule initially interacts with the silicon surface dimer through the formation of a "dative" bond, which occurs with no barrier as the incident gas-phase methylamine molecule approaches the surface, in a manner similar to the ammonia molecule. Once in the "physisorbed," datively bonded well, the methylamine can proceed to react with the surface via a number of pathways. Three of these reaction paths are shown schematically in Figure 2: N−H bond cleavage, N−C bond cleavage, and C−H bond cleavage. The reaction paths shown in the figure are calculated at a low level (HF/3-21G(d)) using the single-dimer cluster surface model and are corrected (scaled) to give the more accurate single-point energy values of the stationary points obtained from the triple-dimer cluster calculations, which are listed in Table 3. This table gives the values for these stationary points after higher level (B3LYP/6-311+G(2d,p)) single-point energy calculations, as outlined in section II. This table also presents the computed values for the related dimethylamine molecule, which has all of these same reaction pathways available to it, as well as results for trimethylamine, which has no N−H bond cleavage path. For comparison, the table also presents previously computed values for these reaction coordinates.[23,24,62] The stationary point energy values computed using the methods outlined in section II are in fairly good agreement with results from more extensive computational approaches and appear to be in good agreement (within about 10 kJ/mol, on average, in the triple-dimer case) with experimentally measured values, where these are known (see section III.C).

Table 3 shows that for all of these molecules the reaction paths out of the dative-bond well present significant (at least 90 kJ/mol, based on the triple-dimer cluster values) barriers to reaction, when measured from the bottom of this well. However, the barrier to N−H bond cleavage is calculated to be below the initial energy of a free molecule and a bare cluster, while the other two barriers, for N−C bond cleavage and for C−H bond cleavage, are both substantially above this level. This ordering of reactive channels for the N−H and N−C bond cleavage channels has previously been noted[23−25] and used to rationalize observed MIR−FTIR results after adsorption of these methylamines on the Si(100)-(2 × 1) surface.[23,24] These studies noted a Si−H stretching feature growing into the spectrum after dosing with either methylamine or dimethylamine with a concurrent reduction of the N−H stretching region to one band (methylamine) or with a disappearance of the N−H stretching feature (dimethylamine). These results indicate that methylamines preferentially react with the silicon surface via N−H bond cleavage. For trimethylamine, the N−H bond cleavage pathway is absent, and this molecule should become trapped in the dative bond well, again consistent with previous MIR−FTIR and photoemission studies.[23,24]

For all of these amines, N−C bond cleavage appears to be the thermodynamically favored final product, followed by N−H bond cleavage, and finally, C−H bond cleavage. However, as mentioned above, the N−C bond cleavage reaction path has a much higher barrier to overcome than the N−H bond cleavage channel, making N−H bond cleavage the kinetically favored reaction route. Inclusion of the possible C−H bond cleavage channel does not appear to alter this energetic ordering. In fact, on the basis of the computational results presented in Table 3, the C−H bond cleavage channel is less favorable than the N−H bond cleavage reaction channel both kinetically (higher barrier) and thermodynamically (shallower well), although it appears to be kinetically favorable compared to the N−C bond cleavage reaction path. The high barrier for C−H bond cleavage is somewhat surprising on the basis of the ease of H transfer for N−H bond cleavage. However, the chemistry of these two reaction paths is quite different. In the case of N−H bond cleavage, the transition state basically involves a proton transfer between the quaternary ammonium-like nitrogen (formal charge +1) in its datively bound state to the electron-rich, nucleophilic "up" silicon atom (formal charge −1) of the dimer.[25] The result is a reduction of the formal charges during and after H transfer. In the case of C−H bond cleavage, a proton is transferred to the "up" silicon atom, negating its −1 formal charge but creating a primary carbanion-like electron distribution around the carbon atom. This "anionic" carbon atom is bonded to the quaternary ammonium-like nitrogen, creating a reasonably unstable zwitterionic species and causing this reaction channel to have a high barrier. Rearrangement (N−Si bond displacement by the carbon) of the zwitterionic amino methyl radical species leads to formal charge reduction and the formation of the Si−C and Si−H bonds of the C−H bond cleavage well.

The N−C bond cleavage reaction path is predicted to be more energetically costly than either of these two H transfer paths. This reaction has been postulated to proceed via a nucleophilic attack on the carbon atom by the "up" silicon atom of the

TABLE 3: Comparison of Results from the Computational Treatment of Amine Adsorption on Si_9H_{12} Single-Dimer and $Si_{21}H_{20}$ Triple-Dimer Clusters as Described in Section II with Previous Computational and Experimental Results[a]

	dative bond well	N−H transition state	N−C transition state 1 (frontside attack)	N−C transition state 2 (inversion)	C−H transition state	N−H well	N−C well	C−H well
			Single Dimer (Si_9H_{12}) Values (kJ/mol)					
			CH_3NH_2					
computations	−94	−32	85	122	81	−220	−288	−172
experiment	−114	−	−	−	−	−201	−	−
Mui et al.[23]	−101	−38	75	−	−	−223	−288	−
Kato et al.[62]	−116	−39	86	−	−	−206	−251	−
			$(CH_3)_2NH$					
computations	−95	−32	94	133	76	−213	−274	−174
experiment	−109	−	−	−	−	−180?	−	−
Mui et al.[23]	−104	−39	81	−	−	−216	−275	−
Cao and Hamers[24]	−113	−27	96	−	−	−212	−263	−
			$(CH_3)_3N$					
computations	−88	NA	101	147	87	NA	−259	−165
experiment	−109	NA	−	−	−	NA	−	−
Mui et al.[23]	−98	NA	91	−	−	NA	−261	−
Cao and Hamers[24]	−104	NA	107	−	−	NA	−248	−
			Triple Dimer ($Si_{21}H_{20}$) Values in kJ/mol					
			CH_3NH_2					
computations	−120	−30	78	108	78	−210	−282	−163
experiment	−114	−	−	−	−	−201	−	−
			$(CH_3)_2NH$					
computations	−123	−18	87	123	72	−206	−267	−162
experiment	−109	−	−	−	−	−180?	−	−
			$(CH_3)_3N$					
computations	−103	NA	108	147	93	NA	−252	−155
experiment	−109	NA	−	−	−	NA	−	−

[a] NA indicates not applicable, and − indicates not measured or calculated.

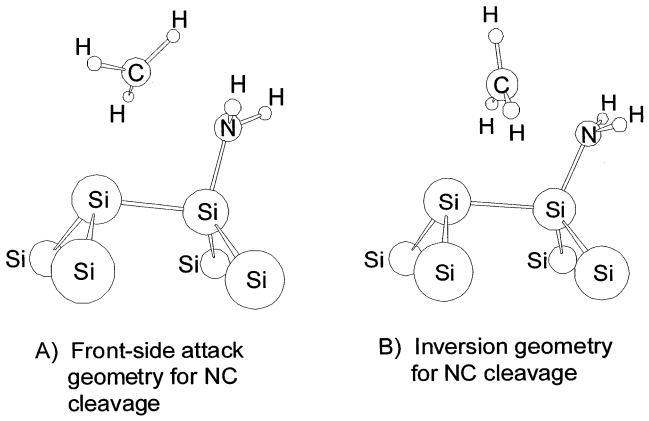

Figure 3. Relative geometries of the "frontside attack" (A) vs "inversion" (B) transition states for methyl group transfer during N−C bond cleavage after methylamine adsorption onto the Si_9H_{12} cluster. The inversion channel is roughly 30 kJ/mol higher in energy than the frontside attack (see Table 3).

dimer.[23] This is energetically more costly than proton-transfer reactions because of both steric (methyl group bulk relative to hydrogen) and electronic (symmetry-forbidden orbital overlap) effects.[23] The transition-state geometry for this nucleophilic attack reveals that the attack occurs via a "frontside" insertion geometry—a path that has been shown to be noncompetitive with the "back−side," inversion attack for gas-phase S_N2 reactions involving ions.[63] The traditional "backside" attack transition state in the case of methylamine lies approximately 30 kJ/mol higher than the frontside geometry (triple-dimer cluster, see Table 3). These two geometries are shown in Figure 3 for clarity. The flipping in the order of these two transition states relative to the gas-phase ion chemistry results, while certainly depending on the exact systems examined, might suggest that under proper geometric constraints, such as when confined to a surface or perhaps more generally in disilene chemistry, frontside nucleophilic substitution reactions can be favored over backside attacks. This might have stereochemical implications for certain S_N2 reactions because the backside attack results in inversion around the carbon center attacked. However, in the case of silicon surface dimers, proton-transfer reactions should dominate for these amines,[25] if this channel is available, and as a result, the "up" silicon atom should act as a better base than nucleophile.

The energetics of an ammonia molecule interacting with an open adsorption site between two adsorbed trimethylamine molecules on the triple dimer cluster were also calculated. The two trimethylamine molecules were adsorbed one each on the two outer dimers of the triple dimer cluster with both of them located on the same "side" of the cluster (the "down" atom in each of these dimers), and the ammonia was allowed to interact with the middle dimer of this cluster but with the silicon atom on the opposite "side" of the cluster (the "down" atom in this dimer). This atom is on the opposite side of the dimer row than the "down" atoms on the outer two dimers of this cluster because the dimers in the dimer row are alternatively buckled up and down. This calculation was aimed at probing the effect of datively bound species on adsorption in the adjacent surface site, which is an indirect probe of the extent of surface delocaliztion of the dative bond. The results for this calculation are given in Table 4, which also shows results for the adsorption of ammonia on a "clean" triple-dimer cluster. These results show that the presence of adjacent trimethylamine molecules destabilizes the interactions of the ammonia molecule with the center dimer by approximately 20 kJ/mol for all of the stationary points (i.e., the datively bound well, the chemisorbed well, and the transition state between these two). This destabilization appears to be electronic in nature, and not steric, because the ammonia

TABLE 4: Comparison of Results from the Computational Treatment of Ammonia Adsorption on the Middle Dimer of a "Clean" $Si_{21}H_{20}$ Triple-Dimer Cluster and a $Si_{21}H_{20}$ Triple-Dimer Cluster with Two Trimethylamine Molecules Adsorbed on the Outer Dimers[a]

	dative bond well	transition state	chemisorbed well
"clean" surface	−123	−21	−209
between two adsorbed trimethylamine molecules	−102	−3	−188

[a] No zero-point vibrational energy (ZPE) corrections were applied in either case (see Table 1 for the ZPE-corrected "clean" dimer adsorption case). Energies are in kJ/mol.

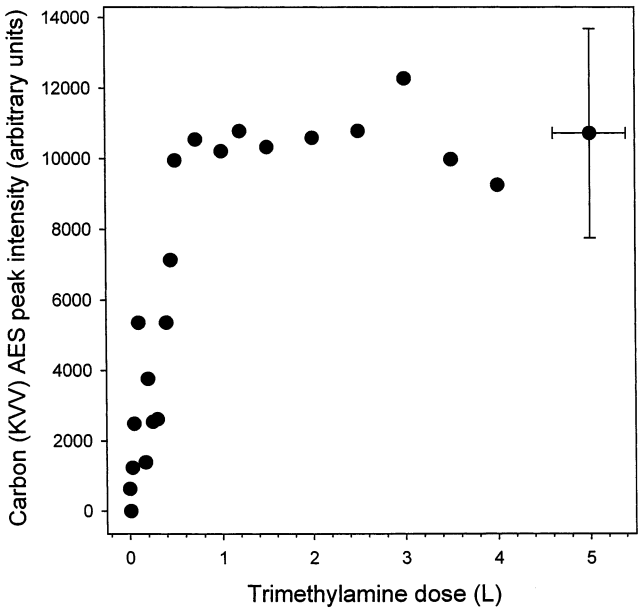

Figure 4. Plot showing the C (KVV) AES peak intensity as a function of trimethylamine dose.

molecule is much smaller than trimethylamine and is located on the opposite side of the dimer row. This delocalization of the dative bonding to adjacent silicon surface dimers manifests itself in the room-temperature surface saturation coverages of these molecules, as has been discussed elsewhere[23] and in the following sections.

B. AES and LEED. Figure 4 shows the uptake of trimethylamine on the room temperature Si(100) surface as a function of trimethylamine dose. The uptake was monitored by observing the AES carbon KVV peak intensity at an electron kinetic energy (eKE) of 273 eV. Plots for dimethylamine and methylamine are very similar in appearance and are not shown. From this figure, it can be seen that the initial uptake of trimethylamine on Si(100) rises rapidly until a dose of about 0.5 langmuir. Above this dose level, the carbon Auger signal remains approximately constant, and it appears that further trimethylamine is not adsorbed on the surface. The coverage at and above this 0.5-langmuir dose level can thus be thought of as the saturation coverage of trimethylamine on the Si(100) surface. For dimethylamine and methylamine the dose required to reach this saturation level is slightly less than that for trimethylamine. To help quantify the amine saturation coverages, the carbon AES signal was calibrated with respect to the AES intensity of a saturated layer of methyl iodide (CH_3I) on the Si(100) surface. The carbon AES signal for trimethylamine saturates at 1.79 ± 0.40 times the signal level for a saturation dose of CH_3I, while dimethylamine and methylamine saturate at 2.21 ± 0.39 and 1.12 ± 0.24 times the CH_3I signal, respectively. Methyl iodide has a room-temperature saturation coverage of 0.43 ± 0.04 monolayers [ML, where 1 ML = 6.78×10^{14} atoms/cm^2 on the Si(100) surface],[64] which indicates that the saturation coverage for trimethylamine is 0.26 ± 0.08 ML on this surface, while dimethylamine and methylamine have coverages of 0.48 ± 0.09 and 0.48 ± 0.11 ML, respectively, based on this comparison. This coverage measurement for dimethylamine is slightly lower than our earlier reported result,[22] although still within the respective experimental uncertainties, because of more precise calibration measurements reported here. Nitrogen Auger signal levels (at 379-eV eKE) showed a similar trend in relative coverage when calibrated with ammonia adsorption[32] but were weaker in intensity and are not shown.

A saturation coverage of 0.26 ML for trimethylamine implies that there is roughly one trimethylamine molecule adsorbed for every four silicon surface atoms (or one molecule per two surface dimers). This AES coverage determination is in good agreement with the 0.24-ML saturation value derived from the integration of N(1s) photoemission intensities as reported by Cao and Hamers,[24] indicating that electron-beam-induced desorption during the Auger analysis is minimal for this molecule. The 0.48-ML saturation coverage value determined for both dimethylamine and methylamine implies one adsorbed molecule for every two silicon surface atoms (one molecule per surface dimer), essentially identical to the 0.50-ML coverage determined for the reaction of the closely related ammonia molecule with this surface.[32] As discussed in section III.A, ammonia is thought to initially interact with the Si(100) surface by the formation of a dative bond via donation of the nitrogen lone pair to one of the surface dimer silicon atoms, followed by NH bond cleavage and transfer of a hydrogen atom to the other silicon atom in the dimer.[32,52−59] This yields NH_2 and H species bound to adjacent silicon atoms of a surface dimer and results in one ammonia molecule adsorbed per dimer. This reaction path is also thought to be available to both methylamine and dimethylamine (see section III.A), consistent with the Auger coverage results. The trimethylamine does not have the NH cleavage channel available, and is thought to be trapped in the dative bond well upon adsorption. The differing coverage value for trimethylamine as compared to ammonia, methylamine, and dimethylamine is an indication that the adsorption chemistry for this species is different from that of these other simple amines.

These AES saturation coverage values can be compared to values obtained for these systems via integration of MIR−FTIR signals as reported by Mui et al.,[23] in addition to the photoemission results of Cao and Hamers.[24] From their IR measurements, Mui et al.[23] estimated that the saturation coverage of dimethylamine is roughly 5−10% less than that of methylamine and that of trimethylamine is only about 25% of the saturation coverage of methylamine. These measurements are somewhat consistent with the AES results, within experimental uncertainty, although the AES saturation value for trimethylamine is closer to about 54% of the saturated methylamine level. However, as Mui et al.[23] point out, quantitative comparisons of integrated IR absorption intensities require knowledge of the absorption cross sections for the comparative modes of each molecule. These cross sections for methylamines adsorbed on silicon are not currently known. However, for methylamine and dimethylamine, the bonding interactions with the surface are expected to be very similar to one another, each molecule having undergone a similar type of addition reaction with the silicon

surface atoms. This might be expected to lead to similar molecular charge distributions and absorption cross sections for these two molecules and, hence, to the relative agreement between the AES and MIR−FTIR coverage measurements. Trimethylamine is not thought to react with the surface via this addition channel and is instead likely to remain trapped in a molecular adsorption well. This should lead to a differing electronic charge distribution within the molecule as compared to that of methylamine and dimethylamine and to differing IR absorption cross sections. AES and photoemission cross sections are not as sensitive to these effects, and this likely accounts for the difference between the AES and photoemission coverage results and the MIR−FTIR coverage results for this molecule.

Low-energy electron diffraction from the room-temperature surface after administering a 2-langmuir dose of trimethylamine shows a two-domain (2 × 1) reconstructed pattern. Methylamine- and dimethylamine-saturated Si(100) surfaces also show this pattern. A (2 × 1) adsorption geometry can be rationalized for molecules having a 0.5-ML coverage on the Si(100) surface; however, a 0.25-ML coverage would likely lead to an adsorbate overlayer having a symmetry of something other than (2 × 1), such as a c(2 × 4) or (2 × 2)-type symmetry, on the (2 × 1) silicon surface. The AES coverage results seem to indicate that a change in diffraction pattern for the different amine-saturated surfaces should be apparent. This is not observed. However, the amine overlayer may not be strongly ordered at room temperature and may not provide a noticeable pattern on top of the diffraction from the underlying, strongly ordered silicon surface. While the exact geometry of the amine adlayers is not readily apparent from the LEED data, the two-domain (2 × 1) LEED patterns do indicate that the underlying silicon dimer σ-bonds are intact after amine adsorption at room temperature, consistent with amine adsorption by either dative bond formation or a 1,2-addition reaction.

C. Thermal Desorption. The major thermal desorption peak observed after room-temperature adsorption of trimethylamine on Si(100) is the parent molecule (m/e = 59 with major QMS ionizer-induced cracking products appearing at m/e = 58, m/e = 42, m/e = 30, and m/e = 15). The peak desorption temperature for this species occurs at 405 ± 20 K. Because the m/e = 58 signal was the most prominent cracking product, it has been selected to represent the desorption of intact trimethylamine. Figure 5 shows a typical desorption trace for the m/e = 58 (parent) desorption channel, along with other observed products at m/e = 2 (molecular hydrogen, peak desorption temperature = 810 K) and m/e = 27 (hydrogen cyanide, peak desorption temperature = about 720 K). Figure 6 shows a plot of the molecular parent peak area (the m/e = 58 signal) vs trimethylamine dose. This plot is very similar in shape to the plot observed for carbon Auger signal vs trimethylamine dose (Figure 4), showing a rapid increase in the parent desorption peak area up to a dose of about 0.5 langmuir, at which point the curve appears to level out. This indicates that the parent desorption channel saturates at approximately the same dose level and surface coverage as the carbon Auger signal. The peak areas for the H_2 and HCN desorption products do not seem to follow as clear a trend vs dose (not shown). However, the HCN signal is quite weak and the molecular hydrogen channel shows a large amount of scatter in the data, and consequently, the experimental uncertainties associated with the measured peak areas would dominate any trend that might exist in these data.

The observation of the trimethylamine parent desorption channel as the major thermal desorption product is consistent with the view that this molecule is trapped in a dative bond

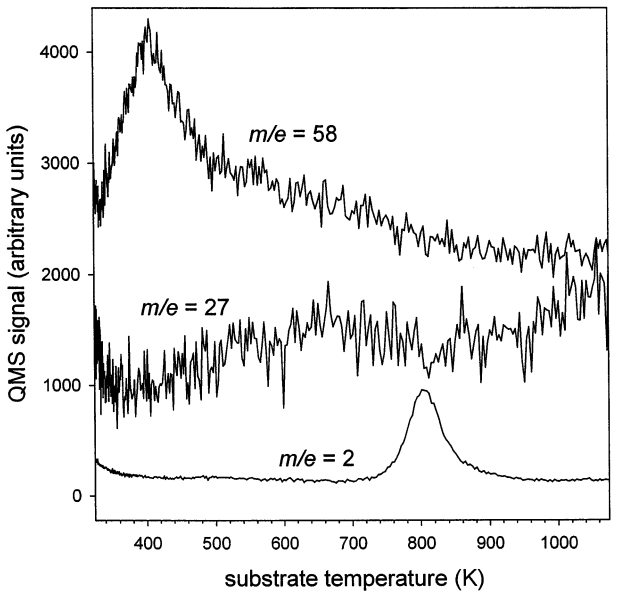

Figure 5. Plot showing the desorption products from thermal desorption of a saturation dose of trimethylamine adsorbed at room temperature on the Si(100)-(2 × 1) surface.

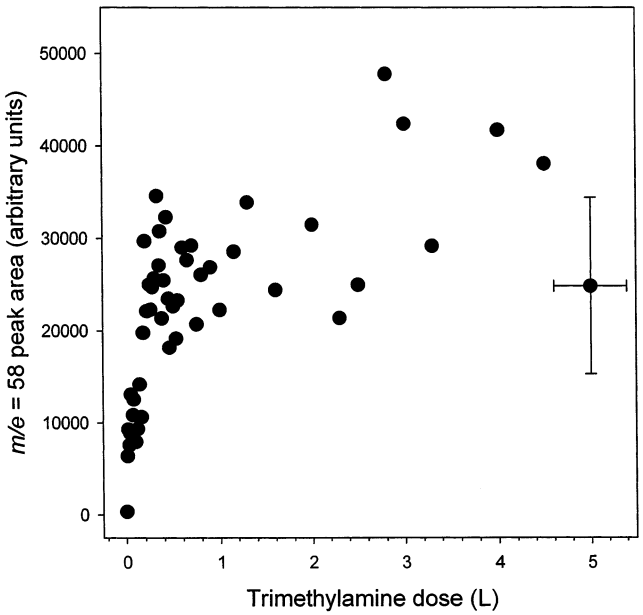

Figure 6. Plot showing the area of the parent trimethylamine desorption peak as a function of trimethylamine dose.

physisorption well on the Si(100) surface and that desorption occurs directly from this well upon heating the surface. The enthalpy of desorption from this well can be obtained from the thermal desorption trace[65] if a few assumptions are made. If first-order desorption kinetics govern this desorption process, the desorption enthalpy can be obtained if one knows the heating rate (2.4 K/s, in this case), the peak desorption temperature (405 K), and the frequency factor for desorption. The computational results on this system from section III.A supply information required to obtain a calculated frequency factor for this desorption reaction. Inspection of the adsorption/desorption curves in Figures 1 and 2 reveals a point in the curve at which the curvature undergoes a distinct change (indicated by arrows in both of these figures). While the curves in these figures are for the ammonia and methylamine molecules, respectively, the curve for trimethylamine is very similar in appearance. If a frequency calculation is done at the geometry of the system

that was obtained at this "kink" point, one finds that this point corresponds to a first-order saddle point (a transition state) with an imaginary frequency of 93 cm^{-1} (in the case of trimethylamine). The normal mode for this motion appears to correspond to a translation of the molecule toward the surface. This "kink" in the desorption curve thus appears to correspond to the point at which the molecule starts to "fall" into the physisorption well from the gas phase (the adsorption or desorption transition state). The ratio of the total partition function (obtained under ideal gas, rigid-rotor, and harmonic oscillator assumptions) for this transition state to the physisorption well partition function (q^*/q) for trimethylamine is calculated to be 2.77 at 405 K. Applying simple transition-state theory then gives a frequency factor of 2.3×10^{13} s^{-1} for this desorption reaction, which gives a first-order enthalpy of desorption of 109 kJ/mol for trimethylamine desorption from Si(100).

The relatively low binding energy for this desorption product is consistent (within about 6 kJ/mol) with the computational treatments of this system (which predict well depths of about 103 kJ/mol [see Table 3]) and indicates that the observed species is produced by direct desorption and not by surface recombination followed by desorption, as has been observed for ammonia adsorbed on this surface.[32] Observation of minor decomposition desorption products in addition to the parent desorption channel is consistent with the photoemission data of Cao and Hamers, who observe that roughly 15% of the molecules on the surface after room-temperature adsorption experience a different bonding environment than the remaining 85%.[24] This is presumably due to N−C bond cleavage, because these authors noted that no peaks appeared to grow into the Si−H stretching region in the IR spectrum and that minor peaks appearing in the photoemission results could be rationalized as arising from the expected products of N−C bond cleavage.[24] From the computational results presented in section III.A, it appears that C−H bond cleavage should be kinetically competitive with the N−C bond cleavage channel, given the 15 kJ/mol lower barrier to reaction. However, it is not clear whether the observed minor channel reaction proceeds over the same dimer N−C bond cleavage barrier that was discussed in section III.A above or through either a channel not calculated for the "ideal" terrace dimer used for the section III.A computations or a channel involving a more complicated surface structure such as a defect, step, or multiple dimer reaction site.

To assess whether the low 0.26-ML saturation coverage of trimethylamine, as determined by AES (section III.B), is a result of steric interactions of the adsorbed molecules on the surface or an electronic effect due to the trapping of these molecules in the dative bond well, as discussed in section III.A, coadsorption experiments with ammonia were performed. Ammonia is much smaller than trimethylamine and, thus, should not suffer the same steric repulsion that a trimethylamine molecule would experience when bonding to a surface dimer site adjacent to a site already occupied by a trimethylamine molecule. However, if this site is empty but has charge delocalization from the adjacent datively bound trimethylamine molecule, the ammonia will likely not be able to bond there at room temperature because the bonding of an ammonia to one of these surface dimers initially proceeds through the same type of datively bound state in which the trimethylamine is trapped.[52] Coadsorption experiments involving both trimethylamine and boron trifluoride on this surface, recently reported by Cao and Hamers,[66] have demonstrated that adsorption of the trimethylamine molecules creates sites of excess electron density on the surface capable of dative bonding to a Lewis acid such as BF_3. These sites of excess electron density are thought to be the silicon atoms in the surface dimers that are not bonded to trimethylamine molecules and are buckled "up" relative to datively bonded silicon atoms. Both the boron trifluoride and trimethylamine showed saturation coverages of about 0.25 ML,[66] consistent with this idea. These ammonia adsorption experiments aim to probe adsorption onto the adjacent (and vacant) surface dimer next to a datively bonded trimethylamine molecule, to probe the amount of dative bond delocalization onto this dimer.

When a surface saturated with trimethylamine was exposed to a "saturation dose" of ammonia (a dose that would cause ammonia saturation of a clean silicon surface) and this doubly exposed surface was subjected to thermal desorption, the resulting ammonia thermal desorption signal (at 695 K, the recombination channel)[32] was approximately 0.14 ($\pm\sim$0.08) times the ammonia signal resulting from an ammonia saturation dose on a clean silicon surface. Similarly, when the surface was exposed to a "two-thirds-saturation dose" of trimethylamine (approximately 0.2 langmuir or about 0.17 ML) and then exposed to a saturation dose of ammonia, the ammonia thermal desorption signal was 0.27 times the clean surface saturation dose signal level. If ammonia could, in an uninhibited fashion, get into the "open" dimers that still exist on the surface after reaction with trimethylamine, then the ammonia signal level for these two cases would be 0.48 [(0.5 ML − 0.26 ML)/0.5 ML or (ammonia saturation level − trimethylamine saturation level)/ammonia saturation level] and 0.66 [(0.5 ML − 0.17 ML)/0.5 ML] times the saturation dose, respectively. If two adsorption sites (i.e., two surface dimers) were blocked for each adsorbed trimethylamine, then the ammonia signals should be 0.04 and 0.38 times the saturation dose for each of these cases, respectively.[67] The ammonia signals are closer to the two sites per adsorbed trimethylamine scenario than to the one site per trimethylamine, even when the surface has a less than complete layer of trimethylamine. This would seem to imply that the site blocking effect for trimethylamine is not due to sterics but is an electronic effect due to the surface accommodation of the dative bond between the trimethylamine molecule and the silicon surface dimer, consistent with the computational results shown in Table 4.

Thermal desorption of methylamine adsorbed to this surface was also examined to compare the reactions of a primary amine with the tertiary trimethylamine molecule. Four main desorption products were noted: $m/e = 2$, 17, 27, and 29. Minor products were also noted at $m/e = 28$ and 31. A thermal desorption trace showing these products (without the $m/e = 28$ product) is shown in Figure 7. The peak areas for all of the observed desorption products follow curves very similar in appearance to the carbon Auger uptake plot for methylamine adsorbed on this surface as a function of dose, showing a rapid increase followed by a leveling off in the signal levels after a dose of about 0.25 langmuir.

The $m/e = 29$ desorption product displayed two peaks, the majority of this species desorbing at 650 K and a minor amount of a species with $m/e = 29$ desorbing at about 870 K. The identity of the major $m/e = 29$ desorption product is believed to be methanimine (CH_2═NH), which corresponds to loss of H_2 from the parent compound. The desorption temperature for this product is close to the 622-K desorption temperature observed for ethene following adsorption of ethyl iodide on this surface.[68] Ethyl iodide is thought to thermally decompose to ethene via a β-hydrogen elimination reaction of the adsorbed ethyl fragment.[69] If methylamine chemisorbs to the surface via N−H bond cleavage, which appears to be the kinetically favored

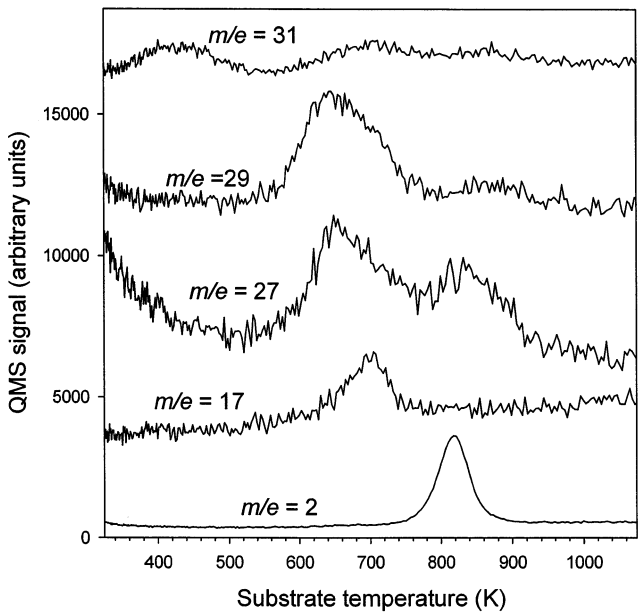

Figure 7. Plot showing the desorption products from thermal desorption of a saturation dose of methylamine adsorbed at room temperature on the Si(100)-(2 × 1) surface.

reaction pathway from computational analyses, the resulting methylamino radical fragment might also be able to undergo a β-hydrogen elimination reaction analogous to that observed for surface-bound ethyl fragments. The resulting unsaturated product would be methanimine. Adsorption of deuterated methylamine (CD_3NH_2) gave thermal desorption products in this temperature range having $m/e = 29-32$, consistent with a species containing three hydrogen atoms (methanimine), although a β-hydrogen elimination reaction mechanism would strictly predict formation of only a species having $m/e = 31$ (CD_2NH) from the presumed CD_3NH surface-bound precursor. This may be an indication that the desorption mechanism for this species is not a simple β-hydrogen elimination reaction, but may also involve some hydrogen scrambling. The minor $m/e = 29$ product desorbing at about 870 K is likely to be due to ethane from recombination of surface methyl groups followed by desorption. This minor product has been noted in previous studies of the decomposition of methyl-containing species on this surface.[22,64,70]

The $m/e = 27$ product displays two peaks at 655 and at 820 K. The first of these appears to be due to ionization-induced cracking of the methanimine species ($m/e = 29$), while the second is likely due to HCN desorption. Hydrogen cyanide is a common thermal decomposition product of amines.[71−75] The $m/e = 17$ product, which desorbed at about 700 K, appears to be NH_3. The 700-K desorption temperature for the $m/e = 17$ product is essentially identical to the temperature observed for the $NH_2 + H$ recombination channel following adsorption of ammonia onto a clean silicon surface.[32] Adsorption of CD_3NH_2 resulted in formation of two main thermal desorption products in this temperature range, $m/e = 17$ (NH_3) and $m/e = 18$ (NH_2D). These results indicate the possible presence of some surface-bound amidogens, which are likely products following either methyl or hydrogen and methylene detachment from methylamine. Analysis of the NH_3 TDS peak area from a saturation dose of methylamine shows that it is about 30% as intense as the NH_3 peak resulting from desorption of a saturation dose of ammonia on this surface. The $m/e = 2$ product, molecular hydrogen, was observed to desorb from the surface at about 820 K, very close to the temperature observed for desorption of hydrogen after water adsorption on the silicon surface.[31] Adsorption of CD_3NH_2 on this surface resulted in the formation of H_2, HD, and D_2 during thermal desorption.

The minor $m/e = 28$ product also displayed two peaks, one at about 650 K and the other at about 870 K; these both appear to be due to ionization-induced cracking of the $m/e = 29$ desorption products. The other minor product ($m/e = 31$) is due to parent methylamine desorption. This product consistently displayed three weak desorption peaks with temperatures of about 430, 720, and ~905 K. When the metallic parts of the sample manipulator were moved into the line of sight of the aperture to the shielded mass spectrometer, the $m/e = 31$ peak at about 905 K was observed to increase in intensity, while both of the other two peaks decreased in intensity. This indicates that this high-temperature methylamine desorption peak originates from the sample holder and not from the silicon sample.

The lowest temperature $m/e = 31$ desorption feature has a desorption temperature very similar to that observed for trimethylamine parent desorption. This is an indication that this methylamine desorption feature also stems from molecular desorption from the physisorbed, dative-bond well. For a first-order desorption process with the observed heating rate of 2.7 K/s and an assumed frequency factor of 1.4×10^{13} s^{-1} (equal to the computed transition-state theory value for methylamine, as discussed above in the case of trimethylamine), the enthalpy of desorption is calculated to be 114 kJ/mol,[65] in good agreement with the computational treatments of this system, which predict a well depth of about 120 kJ/mol (see Table 3).

The amount of parent methylamine trapped in this well after room-temperature adsorption is difficult to estimate because the relative efficiencies for detection of the desorbing species are not known. Static secondary ion mass spectrometry (SSIMS) results by White and co-workers for ammonia adsorbed on Si(100) indicated that undissociated ammonia molecules were present on this surface at room temperature.[53] Assuming that the $SiNH_2^+$ and $SiNH_3^+$ species detected in this study (indicative of surface $-NH_2$ and $-NH_3$ groups, respectively) have similar detection cross sections, the signal level ratios imply a coverage of about 5% molecular ammonia. The interactions of the methylamine molecule (and the dimethylamine molecule) with this surface are expected to be quite similar to those of ammonia, and a comparable amount of parent is likely to be trapped into the physisorbed well. However, in their photoemission study of dimethylamine adsorbed on this surface at room temperature, Cao and Hamers observed only one N(1s) emission peak, falling at a binding energy consistent with a nitrogen atom bonded with silicon following the loss of a hydrogen atom (i.e., not datively bonded).[24] Their data indicate that any datively bonded dimethylamine would be present at a level of about 1% (at most) compared to the dissociatively adsorbed channel.

Even if methylamine is trapped in the datively bonded well upon room-temperature adsorption, one might expect that it would proceed to react with the surface via N−H bond cleavage, rather than desorb, upon heating of the surface because the N−H bond cleavage pathway is predicted to be energetically favored by 30 kJ/mol. The computational results from section III.A indicate that the N−H cleavage path is less favored entropically than desorption by a factor of about 3.7 in the preexponential term. These numbers imply that only about 0.1% of any methylamine trapped in the dative bond well would desorb at 430 K and that most would react via N−H bond cleavage. However, comparison of the computational results for ammonia adsorption on this surface (N−H cleavage favored by 25 kJ/mol, while desorption is favored by a factor of 28.4 in the preexponential term) with experimentally determined values (17

kJ/mol and 33.1)[54] indicates that the computational approach overestimates the stability of the N−H cleavage barrier (by about 47%) and underestimates the relative entropic factors of the two paths (by about 17%). For ammonia, the computational values indicate that at 400 K (the highest temperature at which molecular ammonia SSIMS signal was still observed by White and co-workers)[53] about 1.5% of any physisorbed ammonia would desorb, while the experimental numbers indicate that this value should be closer to about 5%. If these same relative corrections are applied to the methylamine computational results, then about 2% of any datively bonded molecules would be predicted to desorb, the rest reacting via N−H bond cleavage. While this is a small number of molecules that may be desorbing (because it would be about 2% of the trapped molecules, which may be about 1−5% of the molecules on the surface, giving about $(1-5) \times 10^{-4}$ ML overall of desorbing parent), it is consistent with the weak peak attributed to this feature in the thermal desorption traces, although calibration of the exact amount of parent desorbing requires knowledge of the relative ioinization cross sections and detection efficiencies for all of the desorbing species.

Another factor complicating the assignment of this minor desorption channel is that the exact nature of the surface sites where the parent molecule may be trapped is unclear; that is, is the trapping enhanced by defect sites or step sites or does it occur on regular terrace dimers? The signal level for this peak did not significantly depend on the surface preparation technique for the PCA samples because similar signal levels were detected from surfaces prepared either by sputter/annealing cycles or by etching followed by annealing. The VS samples seemed to give rise to a lower (but still detectable and reproducible) signal level for this peak than was observed from the PCA samples. More extensive sample preparation steps were typically required for cleaning of the PCA samples; this could have resulted in surfaces with high defect densities and these sites could act as traps for the datively bonded molecular species. Adsorption of molecular chlorine on the PCA samples, followed by $SiCl_2$ desorption, indicated a surface "missing-dimer" defect density of less than 0.5%, on the basis of comparisons of the low-temperature $SiCl_2$ desorption feature with those found in the literature.[76,77] Surfaces that were miscut by 8° (±0.5°) toward the (111) direction (VS) showed signal levels that were similar to the nominally flat surfaces, even though the step density for the miscut samples should have been higher. The agreement between the derived desorption enthalpy and the computational value for the dative-bond well depth, along with the similarity of this feature to the trimethylamine desorption feature, lends credence to the belief that this feature originates from silicon terrace dimers, although it is not clear from the computational results how much the reaction energetics (or entropics) would change in the vicinity of a surface feature such as a step or another type of surface defect.

The weak 720-K $m/e = 31$ desorption feature appears in the same region as that expected for a hydrogen recombinative desorption channel, as has been observed for ammonia chemisorbed on this surface.[32] If a preexponential factor of 1×10^{14} s^{-1} is assumed for this desorption channel (the same preexponential factor assumed for the recombination channel for molecular ammonia on this surface),[32] the 5.6-K/s heating rate for this portion of the scan and assumed first-order desorption kinetics[65] give a heat of desorption of 201 kJ/mol for this channel. This value is in good agreement with the theoretical predictions for the N−H bond cleavage well depth (about 210 kJ/mol [see Table 3]), indicating that this feature may indeed originate from this recombination channel. While this feature is even weaker than the 430-K desorption feature, it is reproducible and appears to originate from the silicon sample, although the exact nature of the silicon surface features responsible for the appearance of this peak is not entirely clear (i.e., steps, defects, etc.), and an absolute assignment of this feature to the recombination channel for methylamine chemisorbed to this surface cannot be made.

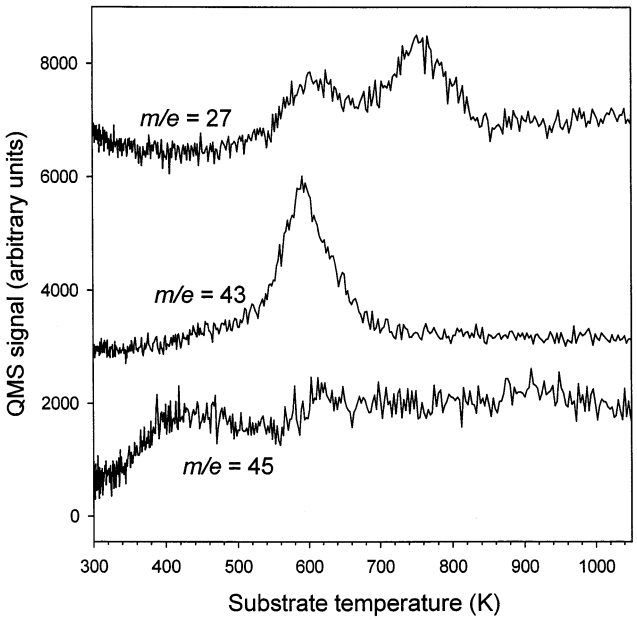

Figure 8. Plot showing the desorption products from thermal desorption of a saturation dose of dimethylamine adsorbed at room temperature on the Si(100)-(2 × 1) surface.

Thermal desorption of dimethylamine adsorbed to this surface was also examined. The reaction of this secondary amine with this surface has been examined previously by our group;[22] however, in the current study, a slightly different distribution of desorbing products is detected compared to that reported in the earlier work. A thermal desorption trace after adsorption of a saturation dose of dimethylamine on the Si(100)-(2 × 1) surface at room temperature is shown in Figure 8. Major desorption products having $m/e = 2$ (not shown), 27, and 43 are noted, along with minor products having $m/e = 28$ (not shown), 29 (not shown), and 45. The production of all of these products versus dimethylamine dose follows plots similar in shape to the AES uptake plots, as is shown in Figure 9 for the $m/e = 43$ product. These show a rapid increase in signal level with increasing dose, followed by a leveling off of the signal levels for doses above about 0.5 langmuir.

The observed thermal desorption products for dimethylamine are very similar in nature to those observed after the interaction of methylamine with this surface. The desorption species having $m/e = 43$ is likely *N*-methyl-methanimine ($CH_3N{=}CH_2$), a β-hydrogen elimination product analogous to the methanimine observed after thermal desorption of methylamine. The peak desorption temperature for this species is about 600 K, again similar to the methanimine desorption temperature. Desorption of hydrogen cyanide ($m/e = 27$) is observed with peaks at 600 and 770 K. The first of these is due to ionization-induced cracking of the $m/e = 43$ species. The final major product observed is molecular hydrogen ($m/e = 2$), which desorbs at 810 K. The minor $m/e = 28$ and 29 products, which both desorb at about 830 K, are likely to be ethane or ethylene resulting from recombination of surface methyls.[22,64,70] The final minor product, with $m/e = 45$, is due to parent dimethylamine

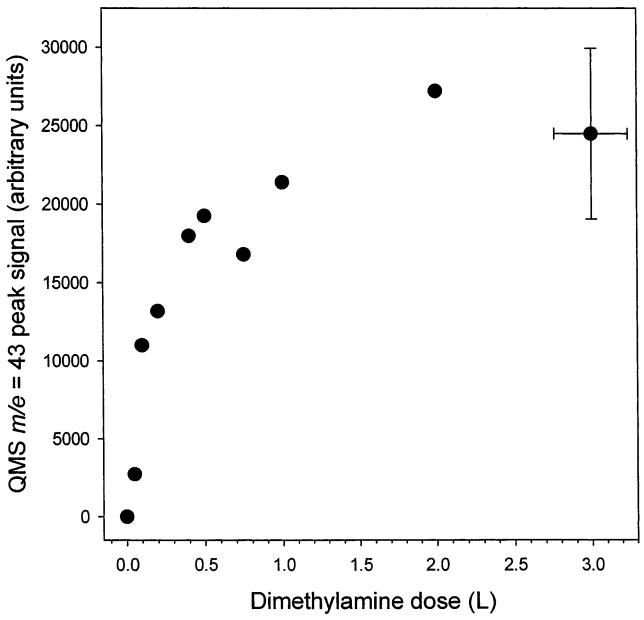

Figure 9. Plot showing the area of the $m/e = 43$ imine product desorption peak as a function of dimethylamine dose.

desorption. This product displays three weak desorption features at 410, 645, and ~950 K. As was the case for methylamine, the higher temperature channel increases in intensity when the metallic portions of the sample holder are moved directly in front of the aperture leading into the shielded quadrupole, while the lower temperature channels decrease in intensity. This indicates that these channels are likely due to parent desorption from the dative bond well (the low-temperature channel), recombination (the middle temperature channel), and desorption from the sample holder (the high-temperature channel). A first-order kinetic treatment[65] for desorption from the dative-bond well, using the observed heating rate for this portion of the temperature ramp of 2.5 K/s and an assumed preexponential factor of 1.6×10^{13} Hz (equal to the computed transition-state theory value for dimethylamine, as discussed above in the case of trimethylamine), yields a heat of desorption of 109 kJ/mol. A similar treatment for the 645-K channel using the 4.9-K/s heating rate for this part of the ramp and an assumed preexponential factor of 1×10^{14} Hz yields a desorption enthalpy of 180 kJ/mol.[65] While the agreement between theory and experiment is good for dimethylamine desorption from the physisorption well (within about 14 kJ/mol, consistent with the methylamine and trimethylamine results [see Table 3]), the agreement for the recombination channel is worse (about a 26 kJ/mol difference, see Table 3). This is an indication that the extremely weak 645-K $m/e = 45$ desorption feature may not be due to recombinative desorption and that assignment as such is tentative at best.

This product distribution and the observation of the $m/e = 45$ product are both somewhat different from the earlier reported results.[22] The current detection of the minor $m/e = 45$ products is likely due to increased sensitivity relative to the earlier study, mainly due to the current tuning of the quadrupole mass spectrometer by sensitivity and mass calibration versus a 20 wt % mixture of five rare gases (He/Ne/Ar/Kr/Xe, Advanced Specialty Gases). The differences between the current and previous $m/e = 43$ production vs dose plots are more puzzling. This discrepancy possibly arises from sample contamination in the previous results. In the previous study, a type-K thermocouple (alumel vs chromel) was used to monitor the sample temperature during heating ramps and was in direct contact with the silicon sample, as well as portions of the sample holder. This caused nickel contamination of the sample,[78] eventually causing enough contamination that the samples exhibited ($2 \times n$) LEED images, indicative of nickel adsorption on this surface.[79] This was not evident during the initial studies of dimethylamine adsorption that were reported in that paper,[22] which still displayed (2×1) LEED images, but it became evident shortly after these studies were completed. However, the samples used in the previous dimethylamine adsorption studies were almost certainly nickel-contaminated to some extent. Even a small amount of this surface contamination can change thermal desorption product distributions, as has been observed for Cl_2 adsorption on nickel-contaminated silicon surfaces.[77] This contamination might also have been responsible for the reduction of the HCN desorption temperature that was observed in this earlier study relative to the current thermal desorption trace (700 vs 770 K). Further confirmation of the effects of surface nickel on the adsorption and reactions of these simple amines is currently being pursued.

IV. Conclusions

The adsorption of several simple methylamines on the Si(100)-(2×1) surface has been investigated using Auger electron spectroscopy (AES), thermal desorption spectroscopy, and low-energy electron diffraction. Both methylamine and dimethylamine appear to undergo mostly dissociative adsorption on this surface at room temperature, although trapping into a molecular adsorption well appears to occur to a limited extent for both molecules, as observed by detection of a parent desorption channel in the 410−430-K temperature range. The major desorbing thermal decomposition product for both of these species seems to come from a β-hydrogen elimination-like reaction of a surface-bound $NH_x(CH_3)_{2-x}$ ($x = 1$ or 0) to form an imine, a reaction that is likely to be analogous to the formation of ethylene from surface-bound ethyl groups.[68,69] This also results in formation of molecular hydrogen, the other main desorbing product observed for both of these species. Trimethylamine, however, appears to undergo mostly molecular adsorption on this surface. By comparison to the AES results from the adsorption of methyl iodide on Si(100), it was concluded that the initial surface saturation coverage of trimethylamine on Si(100) is 0.26 monolayers, while both methylamine and dimethylamine appear to saturate at about 0.48 monolayers. The difference in saturation coverage in the case of trimethylamine appears to be because the molecule is stuck in the physisorption well. This results in blocking of adjacent bonding sites, most likely by delocalized surface electronic accommodation of the trimethylamine−silicon dative bond and leads to a coverage approximately half of that observed for methylamine and dimethylamine. Ab initio and density functional calculations, even at relatively low levels, seem to capture the energetics of these surface reactions within about 15% (about 15−25 kJ/mol) compared to kinetic modeling[65] (using computed and standard frequency factors) of thermal desorption results.

Acknowledgment. Acknowledgment is made to the donors of the Petroleum Research Fund, administered by the American Chemical Society, for partial support of this research. This research was also partially supported by a Research Innovation Award from the Research Corporation and by the University of Nevada, Reno. Additional financial support from the National Science Foundation is gratefully acknowledged under NSF CAREER Award CHE-0094311. J.L.L. was partially supported

by the Research Experiences for Undergraduates program of the National Science Foundation.

References and Notes

(1) Waltenburg, H. N.; Yates, J. T. *Chem. Rev.* **1995**, *95*, 1589−1673.
(2) Hamers, R. J.; Wang, Y. J. *Chem. Rev.* **1996**, *96*, 1261−1290.
(3) Wolkow, R. A. *Annu. Rev. Phys. Chem.* **1999**, *50*, 413−441.
(4) Hamers, R. J.; Coulter, S. K.; Ellison, M. D.; Hovis, J. S.; Padowitz, D. F.; Schwartz, M. P.; Greenlief, C. M.; Russell, J. N. *Acc. Chem. Res.* **2000**, *33*, 617−624.
(5) Bent, S. F. *Surf. Sci.* **2002**, *500*, 879−903.
(6) Buriak, J. M. *Chem. Rev.* **2002**, *102*, 1271−1308.
(7) Bent, S. F. *J. Phys. Chem. B* **2002**, *106*, 2830−2842.
(8) Chadi, D. J. *Phys. Rev. Lett.* **1979**, *43*, 43−47.
(9) Hamers, R. J.; Tromp, R. M.; Demuth, J. E. *Phys. Rev. B* **1986**, *34*, 5343−5357.
(10) Boland, J. J. *Adv. Phys.* **1993**, *42*, 129−171.
(11) Duke, C. B. *Chem. Rev.* **1996**, *96*, 1237−1259.
(12) Hata, K.; Yasuda, S.; Shigekawa, H. *Phys. Rev. B* **1999**, *60*, 8164−8170.
(13) Okazaki, R.; West, R. *Adv. Organomet. Chem.* **1996**, *39*, 231−273.
(14) Veszpremi, T.; Takahashi, M.; Hajgato, B.; Kira, M. *J. Am. Chem. Soc.* **2001**, *123*, 6629−6638.
(15) Eng, J.; Raghavachari, K.; Struck, L. M.; Chabal, Y. J.; Bent, B. E.; Flynn, G. W.; Christman, S. B.; Chaban, E. E.; Williams, G. P.; Radermacher, K.; Mantl, S. *J. Chem. Phys.* **1997**, *106*, 9889−9898.
(16) Bitzer, T.; Richardson, N. V.; Schiffrin, D. J. *Surf. Sci.* **1997**, *382*, L686−L689.
(17) Casaletto, M. P.; Zanoni, R.; Carbone, M.; Piancastelli, M. N.; Aballe, L.; Weiss, K.; Horn, K. *Surf. Sci.* **2000**, *447*, 237−244.
(18) Lopez, A.; Bitzer, T.; Heller, T.; Richardson, N. V. *Surf. Sci.* **2001**, *473*, 108−116.
(19) Ehrley, W.; Butz, R.; Mantl, S. *Surf. Sci.* **1991**, *248*, 193−200.
(20) Casaletto, M. P.; Zanoni, R.; Carbone, M.; Piancastelli, M. N.; Aballe, L.; Weiss, K.; Horn, K. *Surf. Sci.* **2002**, *505*, 251−259.
(21) Zhang, L.; Carman, A. J.; Casey, S. M. *J. Phys. Chem. B*, submitted for publication.
(22) Mulcahy, C. P. A.; Carman, A. J.; Casey, S. M. *Surf. Sci.* **2000**, *459*, 1−13.
(23) Mui, C.; Wang, G. T.; Bent, S. F.; Musgrave, C. B. *J. Chem. Phys.* **2001**, *114*, 10170−10180.
(24) Cao, X.; Hamers, R. J. *J. Am. Chem. Soc.* **2001**, *123*, 10988−10996.
(25) Mui, C.; Han, J. H.; Wang, G. T.; Musgrave, C. B.; Bent, S. F. *J. Am. Chem. Soc.* **2002**, *124*, 4027−4038.
(26) Cao, X.; Hamers, R. J. *J. Vac. Sci. Technol., B* **2002**, *20*, 1614−1619.
(27) Konecny, R.; Doren, D. J. *J. Chem. Phys.* **1997**, *106*, 2426−2435.
(28) Hohenberg, P.; Kohn, W. *Phys. Rev.* **1964**, *136*, B864−B871.
(29) Kohn, W.; Sham, L. J. *Phys. Rev.* **1965**, *140*, A1133−A1138.
(30) Ishizaka, A.; Shiraki, Y. *J. Electrochem. Soc.* **1986**, *133*, 666−671.
(31) Flowers, M. C.; Jonathan, N. B. H.; Morris, A.; Wright, S. *Surf. Sci.* **1996**, *351*, 87−102.
(32) Dresser, M. J.; Taylor, P. A.; Wallace, R. M.; Choyke, W. J.; Yates, J. T. *Surf. Sci.* **1989**, *218*, 75−107.
(33) Kiskinova, M.; Yates, J. T. *Surf. Sci.* **1995**, *325*, 1−10.
(34) Redondo, A.; Goddard, W. A. *J. Vac. Sci. Technol.* **1982**, *21*, 344−350.
(35) Shan, J.; Wang, Y.; Hamers, R. J. *J. Phys. Chem.* **1996**, *100*, 4961−4969.
(36) Roothaan, C. C. J. *Rev. Mod. Phys.* **1951**, *23*, 69−89.
(37) Becke, A. D. *J. Chem. Phys.* **1993**, *98*, 5648−5652.
(38) Lee, C.; Yang, W.; Parr, R. G. *Phys. Rev. B* **1988**, *37*, 785−789.
(39) Frisch, M. J.; Trucks, G. W.; Schlegel, H. B.; Scuseria, G. E.; Robb, M. A.; Cheeseman, J. R.; Zakrzewski, V. G.; Montgomery, J. A., Jr.; Stratmann, R. E.; Burant, J. C.; Dapprich, S.; Millam, J. M.; Daniels, A. D.; Kudin, K. N.; Strain, M. C.; Farkas, O.; Tomasi, J.; Barone, V.; Cossi, M.; Cammi, R.; Mennucci, B.; Pomelli, C.; Adamo, C.; Clifford, S.; Ochterski, J.; Petersson, G. A.; Ayala, P. Y.; Cui, Q.; Morokuma, K.; Malick, D. K.; Rabuck, A. D.; Raghavachari, K.; Foresman, J. B.; Cioslowski, J.; Ortiz, J. V.; Stefanov, B. B.; Liu, G.; Liashenko, A.; Piskorz, P.; Komaromi, I.; Gomperts, R.; Martin, R. L.; Fox, D. J.; Keith, T.; Al-Laham, M. A.; Peng, C. Y.; Nanayakkara, A.; Gonzalez, C.; Challacombe, M.; Gill, P. M. W.; Johnson, B. G.; Chen, W.; Wong, M. W.; Andres, J. L.; Head-Gordon, M.; Replogle, E. S.; Pople, J. A. *Gaussian 98*, revision A.11; Gaussian, Inc.: Pittsburgh, PA, 1998.
(40) Binkley, J. S.; Pople, J. A.; Hehre, W. J. *J. Am. Chem. Soc.* **1980**, *102*, 939−947.
(41) Gordon, M. S.; Binkley, J. S.; Pople, J. A.; Pietro, W. J.; Hehre, W. J. *J. Am. Chem. Soc.* **1982**, *104*, 2797−2803.
(42) Pietro, W. J.; Francl, M. M.; Hehre, W. J.; Defrees, D. J.; Pople, J. A.; Binkley, J. S. *J. Am. Chem. Soc.* **1982**, *104*, 5039−5048.
(43) Hehre, W. J.; Ditchfield, R.; Pople, J. A. *J. Chem. Phys.* **1972**, *56*, 2257−2261.
(44) Gordon, M. S. *Chem. Phys. Lett.* **1980**, *76*, 163−168.
(45) McLean, A. D.; Chandler, G. S. *J. Chem. Phys.* **1980**, *72*, 5639−5648.
(46) Krishnan, R.; Binkley, J. S.; Seeger, R.; Pople, J. A. *J. Chem. Phys.* **1980**, *72*, 650−654.
(47) Frisch, M. J.; Pople, J. A.; Binkley, J. S. *J. Chem. Phys.* **1984**, *80*, 3265−3269.
(48) Pople, J. A.; Krishnan, R.; Schlegel, H. B.; Binkley, J. S. *Int. J. Quantum Chem., Quantum Chem. Symp.* **1979**, *13*, 225−241.
(49) Johnson, B. G.; Frisch, M. J. *J. Chem. Phys.* **1994**, *100*, 7429−7442.
(50) Gonzalez, C.; Schlegel, H. B. *J. Chem. Phys.* **1989**, *90*, 2154−2161.
(51) Gonzalez, C.; Schlegel, H. B. *J. Phys. Chem.* **1990**, *94*, 5523−5527.
(52) Widjaja, Y.; Mysinger, M. M.; Musgrave, C. B. *J. Phys. Chem. B* **2000**, *104*, 2527−2533.
(53) Zhou, X.-L.; Flores, C. R.; White, J. M. *Surf. Sci. Lett.* **1992**, *268*, L267−L273.
(54) Takaoka, T.; Kusunoki, I. *Surf. Sci.* **1998**, *412/413*, 30−41.
(55) Widjaja, Y.; Musgrave, C. B. *Surf. Sci.* **2000**, *469*, 9−20.
(56) Fattal, E.; Radeke, M. R.; Reynolds, G.; Carter, E. A. *J. Phys. Chem. B* **1997**, *101*, 8658−8661.
(57) Loh, Z.-H.; Kang, H. C. *J. Chem. Phys.* **2000**, *112*, 2444−2451.
(58) Lee, S.-H.; Kang, M.-H. *Phys. Rev. B* **1998**, *58*, 4903−4908.
(59) Miotto, R.; Srivastava, G. P.; Miwa, R. H.; Ferraz, A. C. *J. Chem. Phys.* **2001**, *114*, 9549−9556.
(60) Franco, N.; Avila, J.; Davila, M. E.; Asensio, M. C.; Woodruff, D. P.; Schaff, O.; Fernandez, V.; Schindler, K.-M.; Bradshaw, A. M. *J. Phys.: Condens. Matter* **1997**, *9*, 8419−8432.
(61) Ochterski, J. W.; Petersson, G. A.; Montgomery, J. A. *J. Chem. Phys.* **1996**, *104*, 2598−2619.
(62) Kato, T.; Kang, S.-Y.; Xu, X.; Yamabe, T. *J. Phys. Chem. B* **2001**, *105*, 10340−10347.
(63) Angel, L. A.; Ervin, K. M. *J. Phys. Chem. A* **2001**, *105*, 4042−4051.
(64) Gutleben, H.; Lucas, S. R.; Cheng, C. C.; Choyke, W. J.; Yates, J. T. *Surf. Sci.* **1991**, *257*, 146−156.
(65) Redhead, P. A. *Vacuum* **1962**, *12*, 203−211.
(66) Cao, X.; Hamers, R. J. *J. Phys. Chem. B* **2002**, *106*, 1840−1842.
(67) For a saturation dose of trimethylamine on the surface, 0.04 ML are dissociated (15% of 0.26 ML) and 0.22 ML are undissociated (85% of 0.26 ML). If each of these blocks one adsorption site, then 0.26 ML are blocked and 0.24 ML of sites are available for bonding, because one dimer is a bonding site (0.50 ML total sites). If the undissociated trimethylamine molecule blocks two sites, then a saturation dose blocks 0.48 ML (= 0.04 ML + (2 × 0.22) ML) and only 0.02 ML is open for bonding. For a 0.17 ML trimethylamine coverage, 0.03 ML are dissociated and 0.14 ML are undissociated. For one site blocked, 0.17 ML are blocked and 0.33 ML are open. If two sites are blocked by the undissociated trimethylamine, then 0.31 ML are blocked and 0.19 ML are open. Assuming that ammonia can adsorb at any unblocked sites, the ammonia desorption signal levels should be 48% and 66% of saturation signal (0.50 ML) for the 0.26 and 0.17 ML trimethylamine covered silicon surfaces in the one site blocking model and 4% and 38% in the two site blocking model.
(68) Bulanin, K. M.; Shah, A. G.; Teplyakov, A. V. *J. Chem. Phys.* **2001**, *115*, 7187−7195.
(69) Keeling, L. A.; Chen, L.; Greenlief, C. M.; Mahajan, A.; Bonser, D. *Chem. Phys. Lett.* **1994**, *217*, 136−141.
(70) Jackman, R. B.; Chua, L. H.; Foord, J. S. *Surf. Sci.* **1993**, *292*, 47−60.
(71) Loh, K. P.; Kingsley, C. R.; Foord, J. S.; Jackman, R. B. *Surf. Sci.* **1995**, *341*, 92−102.
(72) Somers, J. S.; Bridge, M. E. *Surf. Sci.* **1985**, *159*, L439−L444.
(73) Hamada, Y.; Takeo, H. *Appl. Spectrosc. Rev.* **1992**, *27*, 289−321.
(74) Chen, J. J.; Winograd, N. *Surf. Sci.* **1995**, *326*, 285−300.
(75) Gardin, D. E.; Somorjai, G. A. *J. Phys. Chem.* **1992**, *96*, 9424−9431.
(76) Yang, W.; Dohnalek, Z.; Choyke, W. J.; Yates, J. T. *Surf. Sci.* **1997**, *392*, 8−16.
(77) Dohnalek, Z.; Yang, W.; Ukraintsev, V. A.; Choyke, W. J.; Yates, J. T. *Surf. Sci.* **1997**, *392*, 17−26.
(78) Ukraintsev, V. A.; Yates, J. T. *Surf. Sci.* **1996**, *346*, 31−39.
(79) Kato, K.; Ide, T.; Miura, S.; Tamura, A.; Ichinokawa, T. *Surf. Sci.* **1988**, *194*, L87−L94.